

# Seismic observations of transition zone discontinuities beneath hotspot locations

Arwen Deuss

## Abstract

The seismic structure of the transition-zone discontinuities was studied beneath the 49 hotspot locations of the catalog of Courtillot et al. (2003), using a global data set of SS precursors. Some of these hotspots are proposed to originate from plumes rising in the upper mantle or from the core mantle boundary region. I found thin transition zones in approximately two thirds of the 26 hotspot locations for which precursor observations could be made. This observation agrees with the expectation for the olivine phase transition, of a systematically thin transition zone in high temperature regions. Other hotspot locations showed a clear deepening of both the 410 and 660 km discontinuities, which is consistent with a phase transition from majorite garnet to perovskite at 660-km depth. Predictions from mineral physics suggest that this transition is more important than the olivine phase transition in regions with high mantle temperatures. So, a hotspot location with a deep 410 km discontinuity in combination with either a shallow or deep 660-km discontinuity might be consistent with hot upwellings rising from the lower into the upper mantle. Hotspot locations with a shallow 410-km discontinuity are not in agreement with a positive thermal anomaly from the surface down to the mantle transition zone. This new interpretation of seismic discontinuities in the transition zone has important implication for our understanding of geodynamics in potential mantle plumes locations.

## 1 Introduction

Hotspots (melting anomalies) at the Earth's surface are often attributed to hot thermal plumes in the mantle underneath (Morgan, 1971). While hot upwellings are essential features of mantle convection, it is not necessarily the case that all hotspots are caused by mantle plumes. Alternative explanations have been proposed, such as propagating cracks, abandoned ridges, or other examples of thinned lithosphere above a partially molten mantle (e.g. Anderson, 2000, and see <http://www.mantleplumes.org>). It is important to determine which hotspots are due to deep mantle plumes, and which might

be the result of shallow processes.

The depth of origin of the hotspots is also widely debated. Geochemical data suggest that some hotspots, such as Hawaii, arise from the lower mantle (e.g. Hofmann, 1997). The issue is further complicated by the fact that it has been difficult to image narrow plumes using seismic tomography (Nataf, 2000). While subduction zones are close to seismically active plate boundaries and show up as high-wave speed anomalies, narrow low wave-speed anomalies are not major features in global tomographic models. Nevertheless, some recently developed global models show evidence for vertically continuous negative wave-speed anomalies beneath a few hotspots, extending from the Earth's surface down to either the transition zone or the Core Mantle Boundary (CMB) (Ritsema et al., 1999; Montelli et al., 2004, 2006). There have also been a number of regional studies, for example in Iceland (Foulger et al., 2000, 2001). In locations where the tomographic models suggest that the hotspot is due to a mantle plume, it is also important to obtain constraints on the depth extent of the mantle plume (i.e. upper or lower mantle) using the seismic structure of the transition-zone discontinuities.

Courtillot et al. (2003) suggested five possible criteria to determine if a hotspot has a very deep origin. These include: (1) long-lived tracks, (2) traps or flood basalts at their initiation, (3) high bouyancy-flux values, (4) high  $^3\text{He}/^4\text{He}$  isotope ratios and (5) anomalously low shear-wave speeds. Here, I propose the detailed structure of the transition zone as an additional criterion. This criterion has been used before (e.g. Shen et al., 1998; Li et al., 2000, 2003a,b), but I show that its interpretation is more complicated than was previously thought.

The transition zone separates the Earth's upper mantle from the lower mantle, and is bounded by discontinuities at about 410- and 660-km depths. The characteristics of these discontinuities, such as their depths and wave-speed jumps, are determined by the local temperature and composition. Thus, detailed studies of the transition-zone discontinuities can be used to study lateral variations in temperature and composition of the Earth's mantle. Mantle plumes, with higher temperatures than those in the surrounding mantle, should affect the detailed structure of the transition-zone discontinuities. Most seismic studies of transition zone structure base their interpretation on phase transitions of olivine (Shearer, 2000; Helffrich, 2000), for which the transition zone is thinner in hotter regions and thicker in colder regions. Previous searches for evidence of high temperature anomalies underlying hotspots looked for evidence of a thinner transition zone in these locations (see, for example, Li et al. (2003a,b)).

A recent seismic study of the 660-km discontinuity suggests that mineral phase transitions in garnet must be taken into account in its interpretation (Deuss et al., 2006). The

effects of the multiple phase transitions in olivine and garnet are most pronounced at high temperature (Weidner and Wang, 1998; Hirose, 2002). In particular, the 660-km discontinuity becomes deeper in hotter regions. In combination with a deepening of the 410-km discontinuity at high temperature, the effect of garnet is to leave the transition-zone thickness in hot regions unaffected (Figure 1). Ponding of plume material beneath the 660 km discontinuity could also take place, which would enhance the thermal effects of the positive temperature anomaly on the depth of the 660-km discontinuity.

Here, I use precursors to the seismic phase SS to study the transition-zone thickness in potential high-temperature regions in detail, by focussing on hotspot locations. To do this, I measure transition-zone thicknesses for all these locations and compare the results with predictions based on recent information about the phase diagrams of garnet-olivine mixtures. I also compare my results with locations where seismic tomography models find vertically continuous negative wave-speed anomalies in the upper mantle.

## 2 SS precursors

A global data set of SS precursors was used. This type of data has been used extensively in previous studies to determine the global characteristics of the transition zone discontinuities (e.g. Shearer, 2000). The precursors arrive before the major SS shear wave because they are reflected not from the Earth’s surface but from a discontinuity below the bouncepoint of the SS wave (Figure 2). Precursors are named SdS, where  $d$  is the depth of the reflector. SS precursors are useful for probing the mantle discontinuities globally, beneath both oceans and continents.

SS precursors have a complex Fresnel zone of about 1000 km (Neele et al., 1997). The large size of the Fresnel zone can lead to underestimates in discontinuity topography, in particular if the topography has a smaller wavelength than the Fresnel zone. Mantle plumes are predicted to be quite narrow features, potentially much smaller than the Fresnel zone of the SS precursors. Receiver functions would be more suitable than SS precursors, as they have smaller Fresnel zones, and they have been used before to investigate transition zone discontinuities around hotspot locations (Shen et al., 1998; Li et al., 2000, 2003a).

Unfortunately, many oceanic receiver functions are not located directly above hotspot locations and only a few hotspots have been studied using this technique. SS precursors are the only data currently available with a good global coverage in the oceans to enable a study of all hotspot locations. Model S20RTS shows continuous low wave-speed features, that might be associated with mantle plumes, of sizes comparable or larger than

the Fresnel zones of the SS precursors. Also, the recent shear wave velocity model of Montelli et al. (2006) shows slow features with radius of more than 500 km in certain regions. Thus, mantle plumes are potentially much wider features than has previously been thought, justifying the use of a global data set of SS precursors to search for seismic signatures of potential mantle plumes beneath hotspot locations.

The data were collected from earthquakes in the Incorporated Research Institutions for Seismology (IRIS) catalogue and included all events with depths of less than 75 km and magnitude  $6.0 \leq M_w \leq 7.0$ . This yielded 1625 events with an epicentral distance range of  $100^\circ \leq \Delta \leq 160^\circ$ . Arrival times were measured using cross correlation with a reference pulse, to ensure that only high-quality data were included and to determine the polarities of the SS phases. The selected data set contained 8054 seismograms. These seismograms were band-pass filtered to pass periods of 15-75 sec, resulting in a Fresnel-zone radius of approximately 1000 km. This is similar to the resolution of global tomographic model S20RTS (Ritsema et al., 1999), which was one of the models used for comparison with my SS precursor observations.

The SS precursors have small amplitudes, only a few percent of the main SS-phase amplitudes, and are often not visible on individual seismograms. Therefore, I stacked large numbers of seismograms to suppress incoherent noise and make the precursors visible. First, the traces were aligned on the arrival time of SS, the polarity was reversed if necessary, and each trace was normalised to its maximum SS amplitude. Then the traces were stacked in the slowness-time domain. The stacks were converted into a trace in which the stacking slowness is time-dependent, the time dependence being chosen to maximise the amplitudes of reflections from a continuous range of depths.

I also determined the robustness of the precursors by computing 95% confidence levels for the stacks using the bootstrap resampling algorithm of Efron and Tibshirani (1991). The 95% confidence levels are the  $2\sigma$  error boundaries around the stacked traces. I only interpreted precursors for which the lower confidence levels are larger than zero. The confidence levels are omitted from the plotted results (e.g. Figure 3) for clarity, but the parts of the stacked trace for which the lower confidence level is larger than zero are coloured to highlight the robust reflectors. The depth of the discontinuity was determined by measuring the travel-time difference between SS ( $t_{SS}$ ) and the precursor SdS ( $t_{SdS}$ ). I used a deconvolution technique to determine the travel time differences, by iteratively deconvolving the precursor time window by the main SS pulse (see Chambers et al., 2005). My measurements were corrected for crustal and mantle structure using the crustal model CRUST5.1 (Mooney et al., 1995) and the shear wave-speed model S20RTS (Ritsema et al., 1999).

### 3 Transition zone observations

I computed SS precursor stacks for all 49 globally distributed hotspots from the catalog of Courtillot et al. (2003), which incorporates the catalog of Sleep (1990) (Table 1). As discussed above, SS precursors have a complex Fresnel zone (Neele et al., 1997), and the plumes could be quite narrow features. In order to get the most favourable situation for detecting mantle plumes, it is necessary to compute the precursor stacks centered around each hotspot location. These stacks should lead to better results than comparing hotspot locations with a global map of transition zone discontinuity observations, as was done by Li et al. (2003b).

The stacks were initially computed in the time domain and the 410- and 660-km discontinuity arrival times are measured as travel time differences with the main SS phase. In order to obtain discontinuity depths, a mantle wave-speed model is needed to convert the travel time differences to depths. In addition, a tomographic velocity model and crustal model are used to correct for local 3D structure. However, this causes the exact discontinuity depths to be dependent on the chosen tomographic model. Therefore, I regarded the time measurements as the ‘raw’ measurements, and the computed and corrected depths as ‘interpretations’.

The stacks are presented here in the time domain because these are the most direct, raw measurements (Figure 3). Of the 49 locations, only 32 showed robust reflectors (within the 95% confidence levels) from the transition-zone discontinuities. The other 17 locations did not have enough observations to give robust results, and are omitted here. The remaining 32 hotspot locations show clear reflections from both the 410- and 660-km discontinuities. In some places, for example Iceland, either the 410- or 660-km reflection is characterised by a double peak. Double or broad peaks could be due to the effect of multiple phase transitions (Simmons and Gurrola, 2000; Deuss and Woodhouse, 2001; Deuss et al., 2006), due to the focussing and defocussing by narrow topographic variations (Neele et al., 1997; Chaljub and Tarantola, 1997), or due to ponding of plume material below the 660-km discontinuity (Vinnik et al., 1997). Detailed seismic modelling will be needed to investigate what is causing the double peaks here, which is beyond the scope of this chapter. The locations with double peaks are shown for completeness in Figure 3, but have not been used to measure discontinuity depths or transition zone thicknesses. Transition zone thickness has been measured for 26 locations. Table 1 shows both the measured time differences and the inferred depths for those locations with single reflections from the 410- and 660-km discontinuities.

The hotspot precursor stacks are a subset of a global data set of SS precursor stacks, which has good data coverage in both continental and oceanic regions. The average values

of  $t_{SS} - t_{S410S}$  and  $t_{SS} - t_{S660S}$  are 156 sec and 228 sec for the global data set. These times are indicated with horizontal lines in Fig. 3, and lead to an average transition zone travel-time difference ( $t_{S410S} - t_{S660S}$ ) of 72 sec, which corresponds to a thickness of 242.5 km and is in agreement with other SS precursor studies (Gu et al., 1998; Flanagan and Shearer, 1998). The average depths corresponding to the 410 and 660 arrival times are 410.1 and 652.6 km. The average times and depths are used in this study to test whether observations in hotspot locations differ from those for the average Earth. It is difficult to determine when a depth is significantly greater than the average. I have chosen not to specify a minimum difference from the average, but to list all my measurements to enable readers to make their own decision. The details of my observations are discussed in the next two sections, and possible interpretations are offered.

## 4 Mineral physical interpretation

The transition-zone discontinuities have usually been interpreted in terms of phase transitions in olivine (Anderson, 1967; Ringwood, 1975; Ito and Takahashi, 1989). A transition from olivine ( $\alpha$ -phase) to a spinel crystal structure ( $\beta$ -phase) occurs at 410 km depth, from spinel to ringwoodite ( $\gamma$ -phase) at 520 km depth, and from ringwoodite to perovskite and magnesiowustite at 660 km depth. The olivine phase transition at 410 km depth has a positive Clapeyron slope (pressure increases with temperature), which leads to a deeper transition in hotter regions. The post-spinel phase transition at 660 km depth has a negative Clapeyron slope, and will lead to a shallower transition depth in hotter regions. Defining the transition zone thickness as the distance between the 410- and 660-km discontinuity depths, predicts thinner transition zones in hotter regions. This is the seismic signature that most previous studies of mantle plumes have sought.

However, olivine phase transitions are not the only ones important in the Earth's mantle; other minerals must be taken into account as well. The commonly used pyrolite mantle model contains 60% olivine and 40% garnet at transition-zone pressures (Ringwood, 1975; Irifune and Ringwood, 1987). Most seismic studies have ignored the influence of garnet when interpreting seismic observations of the transition zone discontinuities. However, recent mineral physics studies suggest that garnet phase transitions play a major role in the detailed structure of the discontinuities at 520 and 660 km (Weidner and Wang, 2000). At 520 km depth garnet transforms to Ca-perovskite and around 660 km depth majoritic garnet changes into perovskite. The majorite phase transition at 660 km depth could be more important than the olivine phase transition at high temperatures (Weidner and Wang, 1998; Hirose, 2002). The majorite phase transition has a positive Clapeyron slope, which would lead to a deeper 660 km discontinuity in

hotter areas, and thus a relatively temperature-independent transition-zone thickness. Figure 4 shows the different phase transitions near 660-km depth.

The 410-km discontinuity is not affected by garnet phase transitions. Water might influence the depth and sharpness of the 410-km discontinuity. Bercovici and Karato (2003) suggested the existence of a potentially global water-rich layer near 400-km depth. However, recent experimental work shows that seismically observable effects of water are only expected at mantle temperatures lower than 1200°C and at water concentrations close to saturation level (Frost and Dolejs, 2006). Mantle plumes are expected to have a much higher temperature than 1200°C, so the effect of water can be ignored. The presence of ferric iron may also play a role in broadening the discontinuity, but is as yet unquantified. I will assume that the olivine phase transition alone describes the effects of temperature on this boundary.

Thus, hot thermal regimes are characterised by a deep 410-km discontinuity, but could have either a shallower (olivine dominant) or deeper (majorite garnet dominant) 660-km discontinuity. The dominance of either olivine or garnet is highly dependent on temperature and the exact aluminium (Al) content of the mantle (Weidner and Wang, 1998) and detailed interpretation can only be made after more mineral physical data become available. Here, I will compare my seismic observations with both interpretations.

The arrival times, depths of the discontinuities and transition-zone thickness are plotted in Figure 5 for the 26 locations with a single reflector from both 410 and 660 km depth. Also shown are horizontal and vertical lines denoting the average values for the discontinuity depths and the transition-zone thickness for the global data set; these lines divide each panel in four quadrants. Previous studies have interpreted the combination of a deep 410-km discontinuity, a shallow 660-km discontinuity (and thus a thin transition zone) as evidence for a high temperature, which corresponds to the measurements in the lower right quadrants only of each panel in Figure 5. However, the combination of a deep 410 km discontinuity with a deep 660-km discontinuity and an average transition zone thickness can also be due to high temperatures. This enhances the field of possible mantle plume observations to both the lower and top right quadrants of each panel in Figure 5. It is important to note that variations in the 410- and 660-km discontinuity depths could also be due to local temperature variations in the transition zone only, and a deep 410-km discontinuity does not necessarily prove the existence of vertically continuous high temperature anomalies. The results in this study should only be interpreted as part of a multi-disciplinary effort to determine if mantle plumes exist beneath hotspot locations or not.

The average value of  $t_{SS} - t_{S410S}$  in the global data set is 156 sec. Nineteen locations

(from a total of 31 locations with simple reflections) have larger time differences than 156 sec (Figure 5a and b). When these differential times are corrected for local mantle heterogeneity and the corresponding depths are computed, 18 hotspot locations still show a deeper 410-km discontinuity than the average depth of 410.1 km, and the depths seem to cluster more (Figure 5c and d). Note that some of these locations have double peaks at 660 km depth, so no measurement of the transition-zone thickness is possible. There are 26 locations with both 410- and 660-km discontinuity observations, which are shown in Figure 5.

The locations with a deep 410-km discontinuity have both shallow and deep 660-km discontinuity observations (Figure 5c). The combination of the 410- and 660-km depths leads to a thin or average transition zone thickness (Figure 5d) in all but one of the locations with a deep 410-km discontinuity. All these estimate locations could be due to a positive thermal anomaly, using the mineral physical interpretation described above; they are labelled with an asterisk in Table 1 and the cluster of these locations is circled in Figure 5c and d. The Easter hotspot is the only exception, having a significantly thicker than average transition zone, which could still be due to a high temperature anomaly if the Clapeyron slope of the majorite garnet transition at 660-km depth is larger than the Clapeyron slope of the olivine transition at 410-km depth. If this is indeed the case, then the Easter hotspot will have the largest positive thermal anomaly of all 13 potential mantle plume locations. The remaining 13 hotspot locations with shallower 410-km discontinuities either are not due to positive thermal anomalies in the transition zone, or have thermal anomalies too narrow to be imaged using SS precursors.

The depth of the 660-km discontinuity offers a new method for measuring temperature. Assuming that depth differences are caused only by temperature differences (ignoring compositional heterogeneity), then the locations with the deepest 660 km discontinuities should have the highest temperatures (Figure 4). These locations are in the part of the phase diagram where the majorite-perovskite transition, which has a positive Clapeyron slope, is dominant. Locations with a shallow 660-km discontinuity might still be in the olivine-dominated part of the phase diagram and therefore have lower temperatures. Thus, locations in the top right quadrants of Figure 5a and c could be due to higher temperatures than those in the bottom right quadrants. Easter hotspot, which has the deepest 660 km discontinuity, would then have the largest positive temperature anomaly.

It is important to realise that only about two thirds of the hotspot locations show a deep 410-km discontinuity and the other one third shows a shallow 410-km discontinuity. These measurement do not provide statistically significant evidence for wide high temperature anomalies in the transition zone beneath hotspot locations; from these data alone it is not possible draw conclusions either in favour of or againts the existence of

mantle plumes. The discontinuity measurements presented here should only be interpreted in combination with other geophysical and geochemical data sets, and in particular with other seismological results such as tomographic models (see below).

## 5 Comparison with seismic tomography

Vertically continuous negative shear wave-speed anomalies in the upper mantle, expected for plumes, have been found in some recent global tomographic models (Ritsema and Allen, 2003; Montelli et al., 2004, 2006). A vertically continuous negative shear wave-speed anomaly in the upper mantle below a hotspot will lead to larger-than-average travel time measurements ( $t_{SS} - t_{S410S}$ ) for both the 410- and 660 km reflections in SS precursors, even if there is no deepening of the discontinuities. A large  $t_{SS} - t_{S410S}$  could be due to a deep 410-km discontinuity, or to a low shear-wave speed in the mantle above, or a combination of both. When using a tomographic model to correct SS precursor times for local 3D structure, the large  $t_{SS} - t_{S410S}$  times will be reduced by the correction procedure if the 3D tomographic model has a negative wave-speed anomaly. It is difficult to separate these two competing possibilities, especially as the corrections are sensitive to the specific tomographic model. Therefore, the measurement of absolute discontinuity depths in supposedly hot areas, which will have both a negative wave-speed anomalies and deep 410-km discontinuities, is complicated. Here I will compare the SS precursor observations with two recent shear wave tomography models. Bouyancy flux (Sleep, 1990) is also included in Table 1 for comparison with the SS precursor observations.

### 5.1 Global shear wave model S20RTS

Model S20RTS (Ritsema et al., 1999) is obtained using shear waves, surface waves, and normal-mode splitting functions. It has a horizontal resolution of about 1000 km, which is similar to that of my SS precursor data set, making comparison with my shear-wave observations straightforward. Vertically continuous negative shear wave-speed anomalies in the upper mantle down to the transition zone are present only beneath Afar, Bowie, Easter, Hawaii, Iceland, Louisville, McDonald and Samoa (Ritsema and Allen, 2003). A number of other hotspot locations, on or nearby mid-oceanic ridges, show negative shear wave-speed anomalies in the upper 200 km only, see Table 1. The remaining hotspot locations are without a negative wave-speed anomaly in the underlying upper mantle.

For the hotspot locations with negative wave-speed anomalies in the transition zone, I find large  $t_{SS} - t_{S410S}$  from the 410-km discontinuity in most cases (e.g. Bowie, Easter, Louisville, MacDonald and Samoa). After correcting these arrival times using model

S20RTS and computing the corresponding depths, these locations still have deeper than average 410-km discontinuities. Of the remaining three locations, Afar does not show robust SS precursor reflections, Iceland has an average 410 arrival time, and Hawaii has an early arrival time. Bowie, McDonald and Samoa also have a thin transition zones. Easter has a deep 660-km discontinuity, which might also be consistent with a high temperature if the garnet phase transition is dominant in this location. Louisville shows a double reflection around 660-km depth and no interpretation can be made. It is promising that two different methods with similar resolution, i.e. precursor observations of transition zone discontinuities (this study) and global tomography (Ritsema and Allen, 2003), find evidence for mantle plumes in a number of the same locations.

## 5.2 Finite-frequency model PRI-S05

Montelli et al. (2004, 2006) derived a compressional and a shear wave-speed model using finite-frequency kernels, from which they claimed that a number of hotspots have deep (i.e. lower mantle) or CMB origins. While the significance of finite frequency kernels as compared to ray theory has been disputed (van der Hilst and de Hoop, 2005), comparison with these tomographic results is included for completeness. Table 1 includes the interpretation of Montelli et al. (2006) of the depth origin of mantle plumes below hotspot locations for which robust SS precursor observations were made in this study. The horizontal resolution of model PRI-S05 is in the order of a few 100 km, which is much smaller than the resolution of model S20RTS and the SS precursor observations. It is likely that small scale features of model PRI-S05 cannot be seen in the SS precursor data due to averaging over large areas.

Azores, Cape Verde and Canary all have a shallow 410 km discontinuity, and thus no evidence for a positive thermal anomaly. These hotspot locations show quite narrow plumes in the images of Montelli et al. (2006), so either the potential mantle plumes are too narrow to be seen with the SS precursors or there is no positive thermal anomaly present beneath these locations. Crozet and Kerguelen show a large low wave-speed anomaly near the core-mantle boundary and are interpreted as deep plumes in PRI-S05. These hotspot locations show a thin transition zone but have a shallow 410-km discontinuity and are therefore not interpreted as deep mantle plumes in the SS precursor study.

Bowie, Juan de Fuca and Yellowstone are characterised by shallow, broad low wave-speed anomalies down to the mid mantle, which are quite wide in the transition zone. The SS precursors for Bowie and Juan de Fuca show deepening of the 410 km discontinuity and a thin transition, and are identified as potential mantle plume locations. Yellowstone has

a much lower wave-speed anomaly in PRI-S05 than Bowie and Juan de Fuca. Dueker and Sheehan (1997) found a deepening of the 410-km discontinuity below the Yellowstone hotspot using receiver functions, and that the 660-km discontinuity topography was unrelated to the 410-km discontinuity. There is an ambiguity in the SS precursor observations for Yellowstone, as it has a large  $t_{SS} - t_{S410S}$ , but after correcting for 3D structure the discontinuity depth is shallow. Model PRI-S05 also shows an ambiguity, and this hotspot has not been included in the table of Montelli et al. (2006).

Samoa, Cook Island (close to MacDonald in my table) and Tahiti are closely spaced and have strong low wave-speed anomalies that seem to originate from the Pacific superplume. All three locations are also identified as potential mantle plume locations in the SS precursor study. Tahiti is the strongest plume in model PRI-S05, and has a deep 410 and 660 km discontinuity in the SS precursor observations, in agreement with a large positive thermal anomaly in the mantle transition zone. Samoa has a deep 410 km discontinuity and a thin transition zone. MacDonald is not mentioned in Montelli et al. (2006)'s table, but its location is very close to Cook Island and the SS precursors show a deep 410-km discontinuity and thin transition zone in agreement with a positive thermal anomaly.

Easter hotspot has low wave-speed anomaly in model PRI-S05 which is quite wide in the transition zone, extending down to the core-mantle boundary. The SS precursor data for this hotspot show a deep 410-km discontinuity and the deepest 660-km discontinuity, suggesting the presence of a large positive thermal anomaly in the transition zone. Easter hotspot is one of the few hotspots that is common on the lists of 'major' or 'CMB' hotspot by Courtillot et al. (2003), Ritsema and Allen (2003) and Montelli et al. (2004, 2006), so it is encouraging that the SS precursor data agree with tomographic models and other geophysical and geochemical data sets.

Hawaii is one of the few hotspot locations that has been investigated in regional seismic studies, which found evidence for a low wave-speed anomaly (Priestley and Tilmann, 1999) and also a thin transition zone (Li et al., 2000). Model PRI-S05 shows a large low wave-speed anomaly in the upper mantle, but in the lower mantle it is not the giant plume that it appears to be from observations such as buoyancy flux. The SS precursor data show no evidence for a positive thermal anomaly (average transition zone thickness and shallow 410 and 660 km discontinuities). The transition zone thickness measurements made using receiver functions by Li et al. (2000) show a plume that is narrower than the SS precursor Fresnel zone, so it perhaps not surprising that this signature cannot be seen in the SS precursors.

Iceland has been the subject of a long debate regarding the existence of mantle plumes,

and has had the advantage of a regional network which has been used in a number of studies. Shen et al. (1998) found a thin transition zone using receiver functions and interpreted this as evidence for a lower mantle origin of the Iceland plume. However, a more recent interpretation of virtually the same data set concluded that there was evidence for a thin transition zone due to a deep 410-km discontinuity, but that the 660-km discontinuity was ‘flat’ beneath Iceland (Du et al., 2006). Model PRI-S05 shows a strong low wave-speed anomaly in the upper mantle, in agreement with regional tomographic models (Foulger et al., 2000, 2001), but this signature disappears below 1000 km depth. The SS precursor data show no evidence for a deep 410 km discontinuity, and the 660 km discontinuity is characterised by a double peak, making it impossible to measure one discontinuity depth. The double peaks could be due to the averaging over a large area in the SS precursor stack, but it is interesting to note that Du et al. (2006) show a broadening of the 660-km discontinuity in some stacks. This effect could be due to the combination of the olivine and garnet phase transitions, but more detailed seismic modelling will be required to fully understand the complexities of the transition zone discontinuity observations beneath Iceland.

## 6 Conclusions

Measurements of the transition-zone discontinuities in the hotspot locations of the catalog of Courtillot et al. (2003) show evidence for late arrivals and deeper-than-average depths for the 410-km discontinuity in about two thirds of the cases. A deep 410-km discontinuity agrees with the predicted deepening of the olivine phase transition in high temperature regimes. Most locations with deep 410-km discontinuities, have shallower or average transition-zone thicknesses and either shallow or deep 660-km discontinuities. Mineral physical information (Weidner and Wang, 1998; Hirose, 2002) suggests that either could be consistent with high temperatures. Using these criteria, about half of the hotspots were identified as possible mantle plume locations. A number of these potential plume locations are consistent with negative wave-speed anomalies in the overlying mantle according to the tomographic models by Ritsema and Allen (2003) and Montelli et al. (2006).

One third of the hotspot locations show a shallow or average 410-km discontinuity depth and no evidence for a thin transition zone. These locations are either not consistent with a positive thermal anomaly in the transition zone, or the anomaly is too narrow to be imaged using SS precursors. It is important to note that SS precursors have large Fresnel zones (approximately 1000 km radius), making it difficult to image narrow plumes. Receiver functions would be sensitive to narrow features of about a 100 km

radius, but unfortunately there are only a few receivers close enough to hotspot locations to be used for such an analysis. Future deployment of ocean bottom seismeters will be needed to obtain more detailed constraints on the seismic observability of thermal signatures in the transition zone discontinuities. It is not possible to use the current data set alone to draw general conclusions in favour or against the existence of mantle plumes. Nevertheless, the results presented here will add another 'column' to the hotspot tables and give further evidence in deciding which of the hotspot locations might be due to mantle plumes.

## **Acknowledgements**

This project was supported by a research grant from the Royal Society. Jeff Gu and Bruce Julian are thanked for constructive reviews, and Gillian Foulger for inviting me to attend the 'Great plume debate' in 2005, which encouraged me to work on this topic.

# References

- Anderson, D. L. (1967). Phase changes in the upper mantle. *Science* , 157:1165–1173.
- Anderson, D. L. (2000). The thermal state of the upper mantle; no role for mantle plumes. *Geophys. Res. Lett.*, 27:3623–3626.
- Bercovici, D. and Karato, S. (2003). Whole-mantle convection and the transition-zone water filter. *Nature* , 438:39–44.
- Chaljub, E. and Tarantola, A. (1997). Sensitivity of SS precursors to topography on the upper-mantle 660-km discontinuity. *Geophys. Res. Lett.*, 24(21):2613–2616.
- Chambers, K., Deuss, A., and Woodhouse, J. H. (2005). Reflectivity of the 410-km discontinuity from PP and SS precursors. *J. Geophys. Res.*, 110(B2):B02301,doi:org/10/1029/2004JB003345.
- Courtillot, V., Davaille, A., Besse, J., and Stock, J. (2003). Three distinct types of hotspots in the Earth’s mantle. *Earth and Planet. Sci. Lett.*, 205:295–308.
- Deuss, A., Redfern, S. A. T., Chambers, K., and Woodhouse, J. H. (2006). The nature of the 660-km discontinuity in earth’s mantle from global seismic observations of PP precursors. *Science* , 311:198–201.
- Deuss, A. and Woodhouse, J. H. (2001). Seismic observations of splitting of the mid-transition zone discontinuity in earth’s mantle. *Science* , 294:354–357.
- Du, Z., Vinnik, L., and Foulger, G. (2006). Evidence from P-to-S mantle converted waves for a flat “660-km” discontinuity beneath Iceland. *Earth and Planet. Sci. Lett.*, 241:271–280.
- Dueker, K. G. and Sheehan, A. F. (1997). Mantle discontinuity structure from mid-point stacks of converted P to S waves across the Yellowstone hotspot track. *J. Geophys. Res.*, 102:8313–8327.
- Efron, B. and Tibshirani, R. (1991). Statistical data analysis in the computer age. *Science* , 253:390–395.
- Flanagan, M. P. and Shearer, P. M. (1998). Global mapping of topography on transition zone velocity discontinuities by stacking of SS precursors. *J. Geophys. Res.*, 103(B2):2673–2692.
- Foulger, G., Pritchard, M., Julian, B., Evans, J., Allen, R., Nolet, G., Morgan, W., Bergsson, G., Erlendsson, P., Jakobsdttir, S., Ragnarsson, S., Stefansson, R., and

- Vogfjird, K. (2000). The seismic anomaly beneath Iceland extend down to the mantle transition zone and no deeper. *Geophys. J. Int.*, 142:F1.
- Foulger, G., Pritchard, M., Julian, B., Evans, J., Allen, R., Nolet, G., Morgan, W., Bergsson, G., Erlendsson, P., Jakobsdttir, S., Ragnarsson, S., Stefansson, R., and Vogfjird, K. (2001). Seismic tomography shows that upwelling beneath Iceland is confined to the upper mantle. *Geophys. J. Int.*, 146:504–.
- Frost, D. J. and Dolejs, D. (2006). Experimental determination of the effect of H<sub>2</sub>O on the 410-km seismic discontinuity. *in review Earth and Planet. Sci. Lett.*
- Gu, Y., Dziewonski, A. M., and Agee, C. B. (1998). Global de-correlation of the topography of transition zone discontinuities. *Earth and Planet. Sci. Lett.*, 157:57–67.
- Helfrich, G. (2000). Topography of the transition zone seismic discontinuities. *Rev. Geophys.*, 38:141–158.
- Hirose, K. (2002). Phase transitions in pyrolitic mantle around 670-km depth: implications for upwelling of plumes from the lower mantle. *J. Geophys. Res.*, 107(B4).
- Hofmann, A. W. (1997). Mantle geochemistry: the message from oceanic volcanism. *Nature* , 385:219–229.
- Irifune, T. and Ringwood, A. E. (1987). Phase transformations in a harzburgite composition to 26 GPa: implications for dynamical behaviour of the subducting slab. *Earth and Planet. Sci. Lett.*, 86:365–376.
- Ito, E. and Takahashi, E. (1989). Post-spinel transformations in the system Mg<sub>2</sub>SiO<sub>4</sub>-Fe<sub>2</sub>SiO<sub>4</sub> and some geophysical implications. *J. Geophys. Res.*, 94:10637–10646.
- Li, X., Kind, R., Priestly, K., Sobolev, S. V., Tilmann, F., Yuan, X., and Weber, M. (2000). Mapping the Hawaiian plume conduit with converted seismic waves. *Nature* , 405:938–941.
- Li, X., Kind, R., and Yuan, X. (2003a). Seismic study of upper mantle and transition zone beneath hotspots. *Phys. Earth Planet. Inter.*, 136(1–2):79–92.
- Li, X., Kind, R., Yuan, X., Sobolev, S., Hanka, W., Ramesh, D., Gu, Y., and Dziewonski, A. (2003b). Seismic observations of narrow plumes in the oceanic upper mantle. *Geophys. Res. Lett.*, 30:doi:10.1029/2002GL015411.
- Montelli, R., Nolet, G., Dahlen, F., and Masters, G. (2006). A catalogue of deep mantle plumes: new results from finite-frequency tomography. *Geochem. Geophys. Geosys. (G3)*, in press.

- Montelli, R., Nolet, G., Masters, G., Dahlen, F., and Hung, S.-H. (2004). Finite-frequency tomography reveals a variety of plumes in the mantle. *Science*, 303:338–343.
- Mooney, W. D., Laske, G., and Masters, G. (1995). A new global crustal model at 5 x 5 degrees: CRUST5.0. *Eos Trans. AGU*, 76:F421.
- Morgan, W. (1971). Convection plumes in the lower mantle. *Nature*, 230:42–43.
- Nataf, H.-C. (2000). Seismic imaging of mantle plumes. *Annu. Rev. Earth Planet. Sci.*, 28:391–417.
- Neele, F., de Regt, H., and VanDecar, J. (1997). Gross errors in upper-mantle discontinuity topography from underside reflection data. *Geophys. J. Int.*, 129:194–204.
- Priestley, K. and Tilmann, F. (1999). Shear-wave structure of the lithosphere above the hawaiian hotspot from two-station rayleigh wave phase velocity measurements. *Geophys. Res. Lett.*, 26:1493–1496.
- Ringwood, A. E. (1975). *Composition and petrology of the Earth's mantle*. McGraw-Hill, New York.
- Ritsema, J. and Allen, R. (2003). The elusive mantle plume. *Earth and Planet. Sci. Lett.*, 207:1–12.
- Ritsema, J., van Heijst, H., and Woodhouse, J. (1999). Complex shear wave velocity structure imaged beneath Africa and Iceland. *Science*, 286:1925–1928.
- Shearer, P. M. (2000). Upper mantle seismic discontinuities. *Geophysical Monograph*, 117:115–131.
- Shen, Y., Solomon, S., Bjarnason, I., and Wolfe, C. (1998). Seismic evidence for a lower-mantle origin of the Iceland plume. *Nature*, 395:62–65.
- Simmons, N. A. and Gurrola, H. (2000). Multiple seismic discontinuities near the base of the transition zone in the Earth's mantle. *Nature*, 405:559–562.
- Sleep, N. (1990). Hotspots and mantle plumes: some phenomenology. *J. Geophys. Res.*, 95:6715–6736.
- van der Hilst, R. and de Hoop, M. (2005). Banana-doughnut kernels and mantle tomography. *Geophys. J. Int.*, 163:956–961.
- Vinnik, L., Chevrot, S., and Montagner, J. P. (1997). Evidence for a stagnant plume in the transition zone? *Geophys. Res. Lett.*, 24:1007–1010.

Weidner, D. J. and Wang, Y. (1998). Chemical- and Clapeyron-induced bouyancy at the 660 km discontinuity. *J. Geophys. Res.*, 103(B4):7431–7441.

Weidner, D. J. and Wang, Y. (2000). Phase transformations: Implications for mantle structure. In Karato, S., Forte, A., Liebermann, R., Masters, G., and Stixrude, L., editors, *Earth's deep interior: mineral physics and tomography from the atomic to the global scale*, volume 117, pages 215–235. AGU Geophysical monograph.

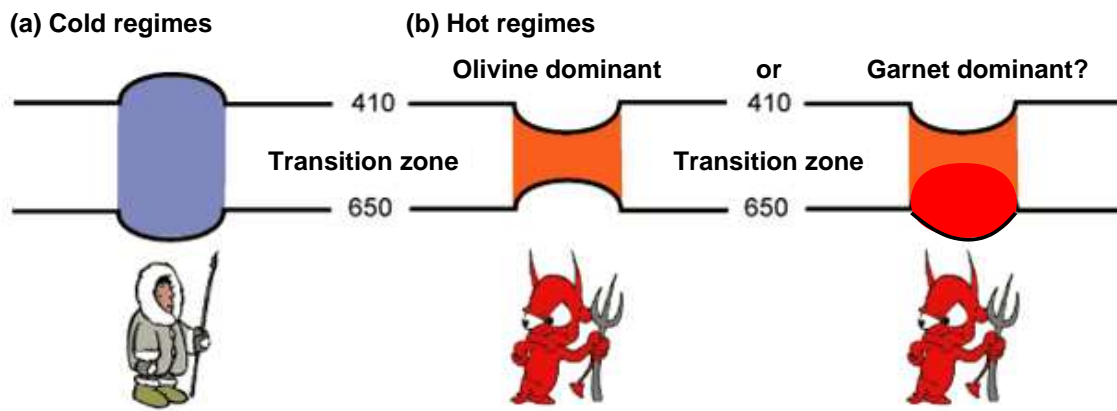


Figure 1: Cartoon showing the different possible behaviours of seismic discontinuities in the transition zone in different thermal regimes, adapted from <http://www.mantleplumes.org>. (a) Olivine phase transitions produce thick transition zones in cold regions (such as subduction zones) and (b) thin transition zones in hot regions (such as mantle plumes). However, garnet might modify the behavior of the 660-km discontinuity in hot regions, leading to lack of anomalies in transition-zone thickness.

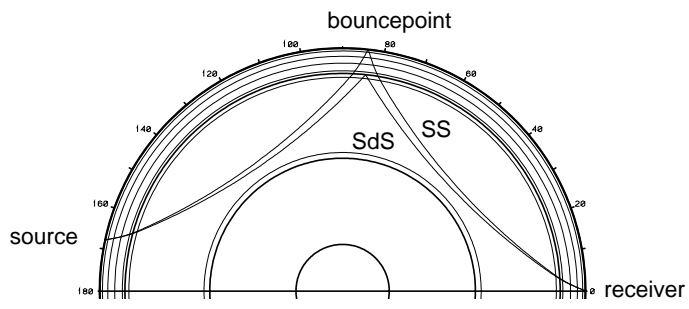


Figure 2: Ray paths of SS (reflected at the surface) and the precursors SdS (here reflected at  $d=660$  km discontinuity).

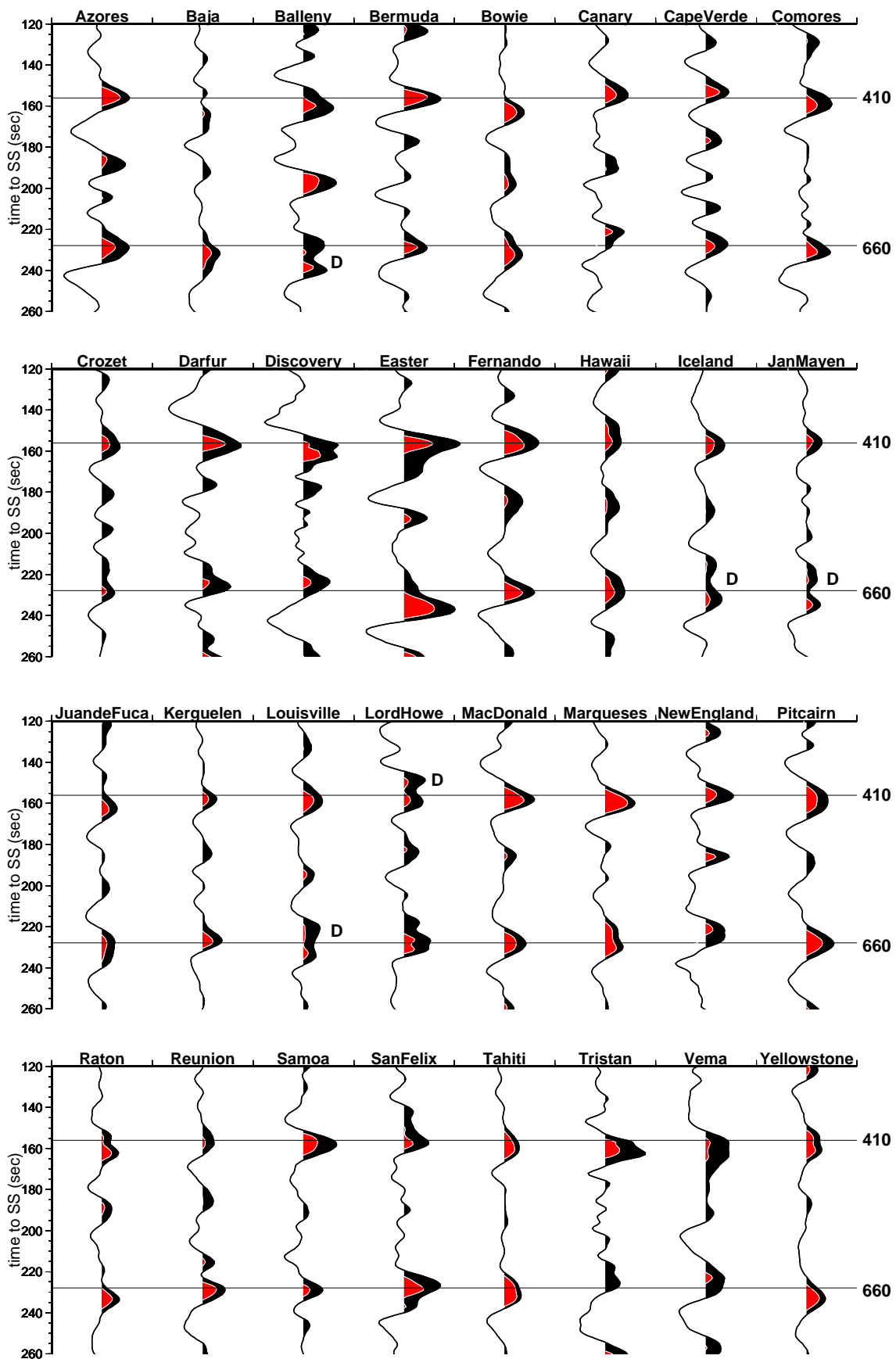


Figure 3: SS precursor stacks for locations of the Courtillot et al. (2003) catalogue. The horizontal lines denote the average arrival times for reflections from the 410- and 660-km discontinuities for the global data set, of which the hotspot locations are a subset. The red coloration shows the area between the lower 95% confidence level and the zero line, denoting robust reflectors. ‘D’ marks the locations with a double peak from the 410- or 660-km discontinuity.

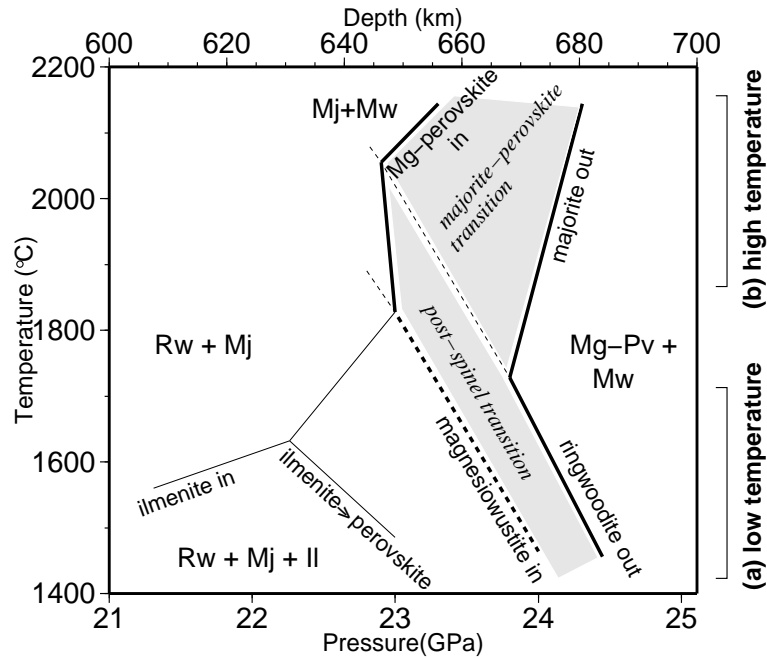


Figure 4: Phase diagram for a pyrolitic mantle at 600 to 700 km depth, after Hirose (2002). The shaded field indicates the perovskite-forming phase transitions that determine the characteristics of the 660-km discontinuity. (a) At low temperatures, perovskite forms from the post-spinel phase in olivine, with a negative Clapeyron slope. (b) At high temperatures, perovskite forms from the breakdown of majorite garnet, with a positive Clapeyron slope. Thin lines show additional phase transitions forming ilmenite and perovskite at shallower depth. Abbreviations are: Rw=rinwoodite, Mj=majorite garnet, Pv=perovskite, Il=ilmenite, Mw=magnesiowustite, Ca-perovskite is also present in all phase fields.

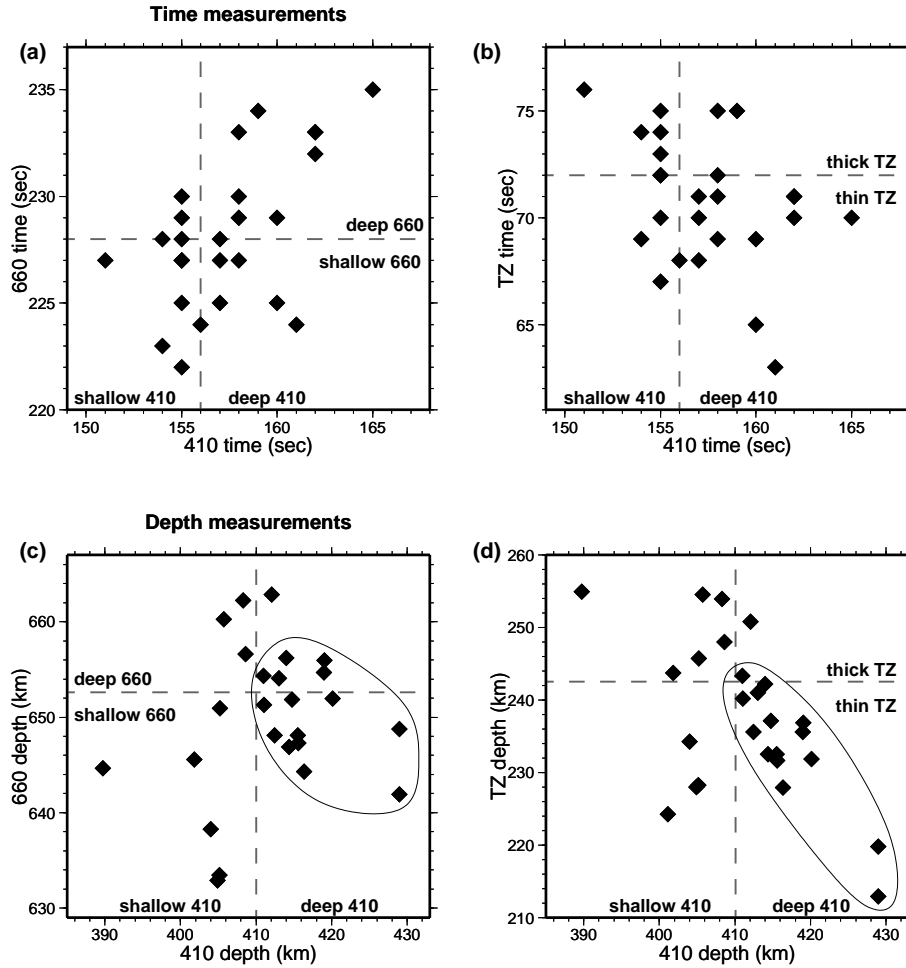


Figure 5: Correlation between the arrival times, depths and inferred transition-zone thickness for the 410- and 660-km discontinuities. Dashed horizontal and vertical lines indicate the average values for our global data set. (a) and (b) show the raw arrival time measurements, (c) and (d) show the computed depths which are corrected for local mantle and crustal structure. The circled clusters are in agreement with the mineral physical signature that would be predicted in potential mantle plume locations, the remaining point in the right top quadrants outside the cluster is Easter hotspot.

Name	Tz (sec)	410 (sec)	660 (sec)	Tz (km)	410 (km)	660 (km)	Tomo S20RTS	Tomo FF	Bouy
Azores	73	155	228	243.7	401.8	645.6	Ridge	d	1.1
Baja*	70	165	235	235.6	419.0	654.7	Ridge		0.3
Balleny		159	D		412.5	D			
Bermuda	72	155	227	241.0	413.0	654.0			1.1
Bowie*	71	162	233	237.1	414.7	651.8	Trans	mm	0.3
Canary	69	154	223	228.2	405.2	633.4		d	1
Cape Verde	76	151	227	255.0	389.7	644.7		d	1.6
Comores*	71	158	229	240.2	411.0	651.2			
Crozet	70	155	225	234.2	404.0	638.2	Ridge	d	0.5
Darfur	67	155	222	224.2	401.2	625.4			
Discovery*	65	160	225	219.8	429.0	648.8			0.5
Easter*	75	159	234	250.8	412.1	662.9	Trans	d	3
Fernando	72	155	227	243.4	410.9	654.3			0.5
Hawaii	74	154	228	245.7	405.2	650.9	Trans	pd	8.7
Iceland		156	D		395.8	D	Trans	d	1.4
Jan Mayen		155	D		399.3	D			
Juan de Fuca*	70	162	232	232.5	415.6	648.1	Ridge	mm	0.3
Kerguelen	68	157	225	228.0	404.9	632.9	Ridge	d	0.5
Louisville		158	D		415.4	D	Trans	pd	0.9
Lord Howe		D	225		D	631.3			0.9
MacDonald*	71	157	228	235.6	412.5	648.1	Trans		3.3
Marqueses*	69	158	227	231.7	415.6	647.3	Ridge		3.3
New England	68	156	224	228.0	416.3	644.3			0.5
Pitcairn*	69	160	229	231.9	420.1	652.0	Ridge		3.3
Raton*	71	162	233	236.9	419.1	656.0			
Reunion	74	155	229	248.0	408.6	656.6		pd	1.9
Samoa*	70	157	227	232.5	414.4	646.9	Trans	d	1.6
San Felix	75	155	230	254.5	405.7	660.2	Ridge		1.6
Tahiti*	72	158	230	242.2	414.0	656.2		d	3.3
Tristan		160			418.4		Ridge		1.7
Vema*	63	161	224	212.9	429.0	641.9			
Yellowstone	75	158	233	253.9	408.3	662.2			1.5
Plume av.	71	157	228	237.2	411.0	648.2			
Global av.	72	156	228	242.5	410.1	652.6			

Table 1: Transition-zone observations from SS precursors using our data set, for hotspot locations from the Courtillot et al. (2003) catalogue. D denotes discontinuities with a double peak, Tz is the transition zone thickness. The locations labelled with an asterix have a deeper inferred 410-km discontinuity in both the measured times and the corrected depths, and have average or thin transition zones. Tomographic information from shear wave velocity model S20RTS is also included, labelled to the depth of the slow velocity anomalies, i.e. ridge or transition zone (Ritsema and Allen, 2003). Interpretations from finite frequency tomography (FF, Montelli et al., 2006) are also included, where d=deep plume, pd=potentially deep, mm=mid mantle. Bouyancy flux is taken from Sleep (1990).